Influence of the Extent of Branching on Solution Conformations of Complex Oligosaccharides: A Molecular Dynamics and NMR Study of a Penta-Antennary "Bisected" *N*-Glycan†

T. J. Rutherford,‡ D. C. A. Neville,§ and S. W. Homans*,‡

Centre for Biomolecular Sciences, University of St. Andrews, St. Andrews, Fife KY16 9ST, U.K., and Department of Biochemistry, University of Dundee, Dundee, DD1 4HN, U.K.

Received June 16, 1995; Revised Manuscript Received September 5, 1995⊗

ABSTRACT: The solution conformation of an agalactosyl penta-antennary "bisected" *N*-linked glycan from hen ovomucoid has been determined using a combination of ^{1}H-NMR NOE measurements and restrained molecular dynamics (MD) simulations. The majority of glycosidic linkages exhibited restricted torsional fluctuations about the global minimum energy configuration, of an extent which was generally less than that observed in *N*-linked glycans with a smaller number of antennae. The locations of terminal galactose residues in the native glycan, which exhibit branch specificity, could not readily be rationalized in terms of relative accessibility by the relevant galactosyltransferase of the various nonreducing terminal 2-acetamido-2-deoxy-D-glucopyranose (GlcNAc) residues in the agalactosyl glycan, suggesting either that the parent protein exhibits substantial control over glycosylation or that more than one transferase is responsible for galactosylation.

N-Glycosylation mediates the biological activity and turnover of many proteins and whole cells [reviewed by Varki (1993)]. The recognition of oligosaccharides and their specificity as acceptors for glycosyl transferases are dependent upon their three-dimensional structure in solution. Glycoform composition is dependent upon the regulated expression of glycosidases and glycosyl transferases, which may vary according to tissue type and stage of development and may be altered in disease states (Takasaki *et al.*, 1980). Knowledge of the conformations of the various glycoforms is a prerequisite for understanding their mode of action and the specificity of their interactions with receptors and glycan-processing enzymes.

Conformational studies have been extensively reported for the lower complex oligosaccharides and their fragments [see Homans (1993) for review]. Key monosaccharide residues exert substantial conformational control which affects the recognition of the oligosaccharide. For example, addition of GlcNAc to the central mannose 4-OH, intersecting the Manα(1→6)[Manα(1→3)]Man branch point, was shown to modify the conformational behavior both of the 6-arm (Brisson & Carver, 1983; Homans *et al.*, 1986) and the 3-arm (Homans *et al.*, 1987). In the current study we have determined the conformation of a penta-antennary "bisected" complex *N*-glycan (**I**, Figure 1) terminating in GlcNAc to investigate the influence of the degree of branching on the overall conformation and to shed light upon the incomplete addition of terminal galactose residues in the native glycan.

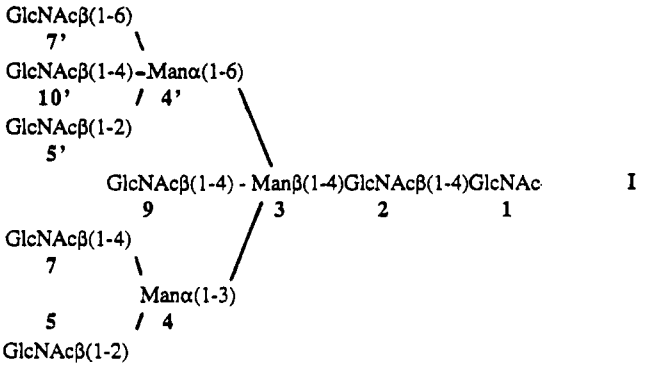

I

FIGURE 1: Structure and residue numbering of the penta-antennary bisected *N*-glycan used in this study.

MATERIALS AND METHODS

Release and Purification of N-Glycan. *N*-Glycans were released from 1 g of hen ovomucoid (Sigma, trypsin inhibitor Type III-O) by preparative scale hydrazinolysis (Patel *et al.*, 1993) and degalactosylated by treatment with 2 units of jack-bean β-galactosidase in 50 mM sodium acetate, pH 5.0, 37 °C, 5 h. The complex mixture of *N*-glycans was separated initially by Bio-Gel P4 gel-permeation chromatography (1 m × 1.5 cm), and the different isomers of biantennary through penta-antennary glycans were purified by high-performance anion-exchange chromatography (isocratic elution with 92 mM aqueous sodium hydroxide, 10 mM sodium acetate through a CarboPac-PA1 column) using a Dionex model BioLC analyzer equipped with a pulsed amperometric detector. The glycan fractions were desalted by passage

† This work was funded by the LINK Biotransformations programme of the Science and Engineering Research Council and the Department of Trade and Industry and by Celltech, Glaxo, ICI, and the Wellcome Foundation. S.W.H. is a Lister Institute Centenary Research Fellow.

* Author for correspondence. Tel.: +44 1334 463795. FAX: +44 1334 463808.

‡ University of St. Andrews.

§ University of Dundee.

⊗ Abstract published in *Advance ACS Abstracts,* October 15, 1995.

[1] Abbreviations: Gal, D-galactopyranose; GlcNAc, 2-acetamido-2-deoxy-D-glucopyranose; HOHAHA, homonuclear Hartmann−Hahn spectroscopy; Man, D-mannopyranose; MD, molecular dynamics; NOE, nuclear Overhauser enhancement; TPPI, time-proportional phase incrementation.

0006-2960/95/0434-14131$09.00/0

through a mixed-bed ion-exchange column (Bio-Rad AG50W-X12 over AG3-X4), dried by evaporation, and exchanged three times in D_2O.

^{1}H-NMR spectra revealed one set of signals for each mannose residue, indicative of no major contamination from other glycoforms. Electrospray mass spectra (in positive mode) of a partially purified mixture of *N*-glycans identified molecular ions for the monosodium adducts of the permethylated penta-antennary glycans (*m/z* 2642.3; expected 2643.9) as the major component and permethylated tetra-antennary glycan (*m/z* 2398.7; expected 2398.7) as a minor component. ^{1}H chemical shifts in the structural reporter group region of the major component were identical to those of the purified glycan used for conformational analysis.

NMR Spectroscopy. ^{1}H-NMR spectra were recorded with a Bruker AM-500 spectrometer (operating at 500.13 MHz), with a nominal probe temperature of 300 K. NOESY spectra were acquired with TPPI for f_1 quadrature, using the standard Bruker microprogram. Spectra were acquired over a spectral width of 2000 Hz with 256 and 4096 data points in t_1 and t_2, respectively. The matrix was processed with cosine-bell apodization in both dimensions using Varian VNMR software. The digital resolution in the final spectrum was 4.0 Hz/point in f_1 and 1.0 Hz/point in f_2. NOE intensities were determined from cross-peak volumes, following fifth-order polynomial base line correction.

Molecular Modeling. The NMR/molecular dynamics (MD) modeling protocol used in this study has been demonstrated to give excellent agreement with experimental data for small oligosaccharides (Rutherford *et al.*, 1993, 1994; Kogelberg & Rutherford, 1994; Rutherford & Homans, 1994). The protocol utilizes *in vacuo* MD simulations which incorporate NOE-derived distance constraints to compensate for the poor performance that is observed for molecular mechanics force fields over the entire range of conformational space. As previously described (Rutherford & Homans, 1994), by applying loose constraints in the form of a flat-bottomed pseudopotential well there is scope for considerable variation between experimental and back-calculated relative NOE values, but in practice excellent correlations are found between theoretical back-calculated values and experimental values, not only for relative NOEs, but also for interglycosidic $^3J_{CH}$ which are independent of the applied constraints (Rutherford *et al.*, 1993, 1994; Kogelberg & Rutherford, 1994). Moreover, in studies to date there are no short interproton distances that are not evident from the NOE spectra. The restrained MD model depicts the minimum conformational space that is compatible with experimental data, but, given that in all studies to date this has included the conformers with lowest potential energy, it is difficult to envisage alternative equilibria that are also compatible with experimental data. The penta-antennary glycan is a highly branched structure, and significant inaccuracies in the modeled conformational equilibria would inevitably result in many short time-averaged H−H distances that could not be confirmed from NMR experiments. This structure therefore represents a rigorous test for conformational modeling procedures.

All modeling calculations were performed using the DISCOVER molecular mechanics package (Biosym Technologies Inc., San Diego, CA) running on an Iris Indigo-4000 computer. Simulations were performed *in vacuo* with a dielectric constant $\epsilon = 80.0$, using the AMBER force field (Singh *et al.*, 1986; Weiner *et al.*, 1986) with the carbohydrate parameter set described previously (Homans, 1990) but with all torsion terms corresponding to the *exo*-anomeric effect set to zero (Rutherford *et al.*, 1993). Initial velocities were assigned at random according to a Maxwell−Boltzmann distribution at 300 K, and the system was coupled to a temperature bath with a time-constant of 0.6 ps. The cutoff distance for calculating nonbonded interactions was 15 Å. NOE-derived distance restraints were applied as symmetrical biharmonic restraints with a force constant of 10 kcal/Å^2 and a maximum force of 10 kcal/Å. Constraints were classified as strong, medium, or weak, with lower and upper distance bounds of 1.8−2.7, 1.8−3.3, and 1.8−5.0 Å, respectively. The modeling protocol was identical to that described previously for oligosaccharides (Rutherford *et al.*, 1993, 1994; Kogelberg & Rutherford, 1994; Rutherford & Homans, 1994), using MD calculations at 750 K to generate 10 starting structures with pseudorandom geometries and annealing the 10 models with NOE constraints (running 1 ps of MD at each temperature from 500 to 300 K in steps of 50 K, then from 290 to 10 K in steps of 10 K and finally at 5 K followed by steepest-descents minimization). The lowest energy model from the annealing simulations was used as the input structure for 510 ps MD simulations at 300 K. MD coordinates were stored after every 250 time steps of 1 fs, and time-averaged full relaxation matrix NOE values were computed from the final 500 ps of archive data using the in-house written program MDNOE, with a formalism appropriate for internal motions that are fast with respect to the overall tumbling time of the molecule (Tropp, 1980; Homans & Forster, 1992). This formalism is implemented using the assumption that the zero-quantum spectral density dominates the cross-relaxation rate [eq 19.1 in Tropp (1980)], which is clearly the case in the present study since all NOEs are significantly negative. In addition, overall isotropic motion of the glycan is assumed, and a single internal correlation time with averaging between N sites is assumed for the internal motions. While a more detailed model for the nature of the internal motion would clearly be more rigorous, in practice the eigenvalues and eigenvectors of the matrix of rate constants describing the motion cannot be specified in general, and it is necessary to approximate motional limits in which these constants drop out in order to calculate the spectral densities analytically (Tropp, 1980). Clearly the relevant spectral densities could be obtained numerically by Fourier transformation of the relevant autocorrelation functions derived directly from the dynamics trajectory, but this would require a simulation including explicit solvent water molecules for a time much greater than is currently computationally tractable for a molecule the size of **I**.

The glycosidic torsion angles ϕ and ψ are defined by the torsion angles H1−C1−O1−C*x* and C1−O1−C*x*−H*x* where C*x* and H*x* are aglyconic atoms and are formally designated ϕ_H and ψ_H in IUPAC nomenclature. For 1→6 linkages ψ_H and ω_H are defined with respect to C1−O6−C6−C5 and O6−C6−C5−H5, respectively. The numbering of residues (Figure 1) follows the convention of Vliegenthart *et al.* (1983).

RESULTS

^{1}H-NMR Assignment. The penta-antennary complex *N*-glycan (**I**, Figure 1) is composed solely of mannose and

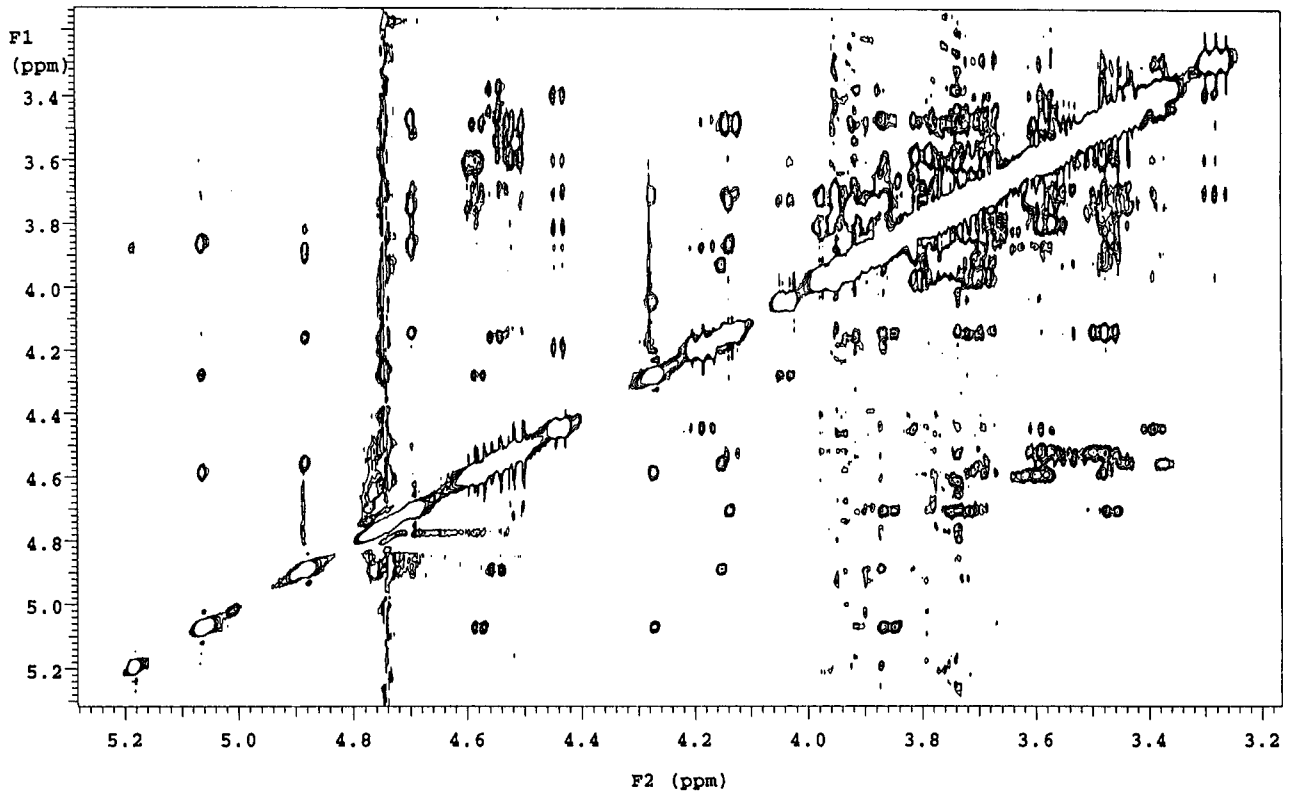

FIGURE 2: $^1H-^1H$ NOESY spectrum of **I** obtained with a mixing time of 300 ms.

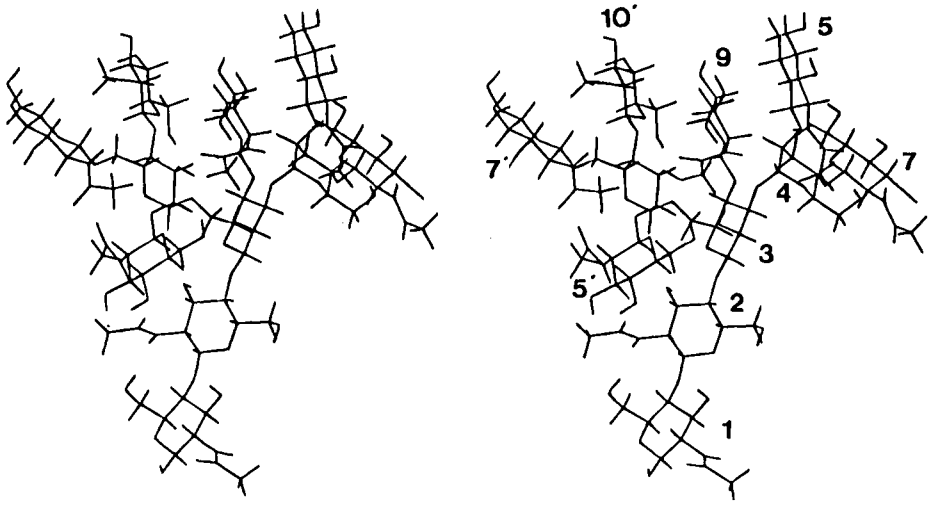

FIGURE 3: Stereoview of the "global minimum" energy configuration of **I** derived from restrained simulated annealing calculations.

N-acetylglucosamine and as might be expected many of the residues have virtually degenerate ^1H spin systems. Assignment of the many overlapping GlcNAc resonances employed HOHAHA experiments with constant-time evolution during t_1, refocussing the H1−H2 spin-couplings in order to maximize resolution in the f_1 dimension, as previously described (Rutherford & Homans, 1995). Approximate $^3J_{HH}$ values measured from the 2D spectra indicated that each ring adopts predominantly the expected $^4C_1$ chair conformation. In a slice parallel to f_2 in the HOHAHA spectrum (not shown), at the Manβ (3) H-4 chemical shift in f_1, the H-5 resonance appears with unresolved spin-couplings to H-6 protons. The only orientation of the hydroxymethyl group in which both $^3J_{H5-H6}$ values are small (~1.5 Hz) (Nishida *et al.*, 1987) is $\omega = 180°$ (the "*gauche−gauche*" or "*gg*" rotamer), consistent with previous reports that the ω angle for the Manα(1→6)Manβ linkage in intersected *N*-glycans is fixed in the *gg* rotamer (Brisson & Carver, 1983; Homans *et al.*, 1986). Stereospecific assignments were made for the two H-6 protons of the Manβ residue on the basis of the NOESY correlation between H-4 and H-6_{proR}.

Previous NOESY time-course experiments with *N*-glycans have indicated that a mixing time of 300 ms is within the linear NOE build-up region, where the measured NOE is directly proportional to the cross-relaxation rate, σ, and the isolated spin pair approximation is valid (Homans *et al.*, 1987). However, in the present study we have utilized a complete relaxation matrix analysis of the data (see below). A total of 24 interresidue correlations were obtained from the NOESY spectrum (Figure 2 and Table 1) and were utilized as distance constraints in the annealing calculations and MD simulations. The modeling constraint between the

Table 1: Experimental Absolute NOE and Values Back-Calculated from Time-Averaged Distances in Restrained and Free MD Simulations for **I**

protons			exptl	calculated NOE (%)[a]	
from	to	constraint	NOE (%)	restrained	free
H-1 (2)	H-4 (1)	S	n.d.[b]	3.0	1.6
H-1 (3)	H-4 (2)	S	11.9[c]	5.0	1.8
H-1 (4)	H-2 (3)	W	1.0[d]	0.4	1.4
H-1 (4)	H-3 (3)	S	8.5	4.0	5.1
H-1 (4)	H-2 (9)	W	1.4	1.3	0.1
H-2 (4)	H-6 (9)	M	4.2	1.0/2.0	0.1/0.1
H-5 (4)	H-2 (3)	S	7.3[c]	4.0	0.3
H-1 (4′)	$H\text{-}6_{proS}$ (3)	S	4.4	3.9	0.6
H-1 (4′)	$H\text{-}6_{proR}$ (3)	M	1.5	1.3	0.4
H-3 (4′)	H-4 (3)	W	1.5	2.5	0.2
H-1 (5)	H-1 (4)	S	5.7	4.1	0.4
H-1 (5)	H-2 (4)	S	4.1	4.7	2.8
H-1 (5)	H-2 (9)	S	3.7[c]	2.7	0.3
H-1 (5′)	H-1 (4′)	S	5.3	2.7	1.0
H-1 (5′)	H-2 (4′)	S	5.6[c]	3.0	1.6
H-1 (7)	H-4 (4)	S	n.d.	3.2	1.5
H-1 (7′)	H-6 (4′)	M[e]	2.6[c]	0.7/1.1	1.5/1.0
H-1 (9)	H-4 (3)	S	5.3	4.0	2.3
H-1 (9)	$H\text{-}6_{proR}$ (3)	M	4.5	1.5	2.0
H-1 (9)	H-3 (4′)	W	1.8	1.2	0.3
H-1 (9)	H-5 (4′)	M	3.6	1.5	0.3
H-4 (9)	H-5 (5)	W	2.7	2.5	0.1
H-1 (10)	H-4 (4′)	S	8.2[c]	3.5	0.4
H-1 (10)	H-6 (4′)	W	n.d.	0.3/0.3	0.1/0.2

[a] Computed with a rotational correlation time, $\tau_c = 1.1$ ns. [b] n.d. = not determined due to extreme resonance overlap. [c] Approximate value due to substantial resonance overlap. [d] Approximate value due to low signal-to-noise ratio. [e] Measured NOE was "strong", but since the assignment of H-6 protons was not stereospecific a weaker constraint was applied to both H-6's.

intersecting GlcNAc (residue 9) and the Manβ (3) $H\text{-}6_{proR}$ was applied stereospecifically, whereas for all other residues hydroxymethyl groups were not restricted to a single rotamer as H-6 protons could not readily be assigned stereospecifically. Modeling constraints involving these H-6 protons treated both H-6 protons together as a pseudoatom.

Molecular Modeling Calculations. Ten models of **I** were generated by high-temperature (750 K) unrestrained molecular dynamics calculations to provide pseudorandom starting structures that sample a wide range of conformational space. Low-energy models were generated for **I** by restrained simulated annealing of pseudorandom starting structures. Due to the imperfect nature of the annealing, one structure was caught in an unrealistic local energy minimum with distorted ring geometries and was discarded. The lowest energy ("global minimum") structure (Figure 3) from the 10 annealed models had a low NOE distance-forcing potential (totaling 0.28 kcal/mol for the 24 constraints), and it is therefore unlikely that the constraints were forcing the model into a high-energy virtual conformation. The lowest energy model was used as the starting point for a 510 ps restrained molecular dynamics (MD) simulation *in vacuo* at 300 K.

In addition to the restrained MD simulation an unrestrained 510 ps MD simulation was performed under otherwise identical conditions. Theoretical time-averaged MD simulations were computed over the last 500 ps of each simulation using a full relaxation matrix approach which considered all nonexchangeable protons, and with a formalism (see Materials and Methods) appropriate for internal motions which are fast with respect to overall reorientational tumbling of the molecule (Tropp, 1980; Homans & Forster, 1992). A comparison of the experimental NOE values with those back-calculated from each MD simulation is included in Table 1. The absolute NOE values were computed as follows. Using a suitable intraresidue NOE (Man 4 H-1−Man 4 H-2), the ratio of diagonal peak to cross-peak volumes was compared with that obtained from the time-averaged full relaxation matrix calculation above, and the overall tumbling time (τ_c) was adjusted in the calculation such that the ratio of theoretical intensities matched those obtained experimentally. The absolute NOE obtained from the calculation was then used to derive the experimental absolute NOEs from the respective cross-peak volumes, using the volume of the Man 4 H-1−Man 4 H-2 cross-peak volume as a reference.

The results in Table 1 indicate that the restrained MD model shows significantly better agreement with the experimental data than the unrestrained simulations. As indicated previously (Rutherford & Homans, 1994), a small error in the simulated distances due to the many inaccuracies inherent in the force field parametrization translate to very large errors in the back-calculated NOEs due to the r^{-6} dependence, and we regard agreement between experimental and back-calculated NOEs within a factor of 2 as satisfactory. The majority of NOEs calculated from the restrained simulation are within or are close to this criterion. In contrast the free dynamics simulations do not reproduce many of the experimental NOE intensities, primarily as a result of torsional excursions for significant periods of time into regions of conformational space divorced from the minimum energy conformation, as seen clearly in Figure 4. These data therefore suggest that a plausible model of the solution dynamics of the glycan is given by the restrained dynamics simulation. A possible criticism of this interpretation is that the derivation of simulated NOE data from a dynamics trajectory which is restrained by experimental NOE data is rather circular. However, as described at length previously (Rutherford & Homans, 1994), the simulated NOE can vary over a wide range despite the presence of restraints, yet good agreement is obtained with experimental values. In any event, the dynamic model generated from a restrained trajectory can be at least interpreted as representing the minimum extent of torsional fluctuation consistent with experimental data. Time-averaged values of ϕ and ψ for each glycosidic linkage over the time course of the restrained simulation are given in Table 2.

The total NOE distance-forcing potential was monitored during a separate restrained MD simulation, in which the calculation was stopped and resumed at 1 ps intervals to record the contributions from each individual term in the force field. The force potential remained low throughout the MD simulation, averaging 0.70 kcal/mol over the 500 ps time course, with a maximum of 3.86 kcal/mol at any one point.

Further evidence for the plausibility of the model can be obtained by consideration of time-averaged NOEs predicted from the simulation which are not observed experimentally. A total of 19 such NOEs are predicted (Table 3). However, since the limit of detection is on the order of 1% NOE (based on the NOE between Man 4 H-1 and Man 3 H-2, which is just detectable), at least 13 of these can immediately be discounted. The NOE between Man 4′ H-2 and Man 3 H-4 (2.6%) cannot be discounted, but, however, it is essentially unobservable experimentally due to the proximity of these proton resonances. The only other NOE which is substan-

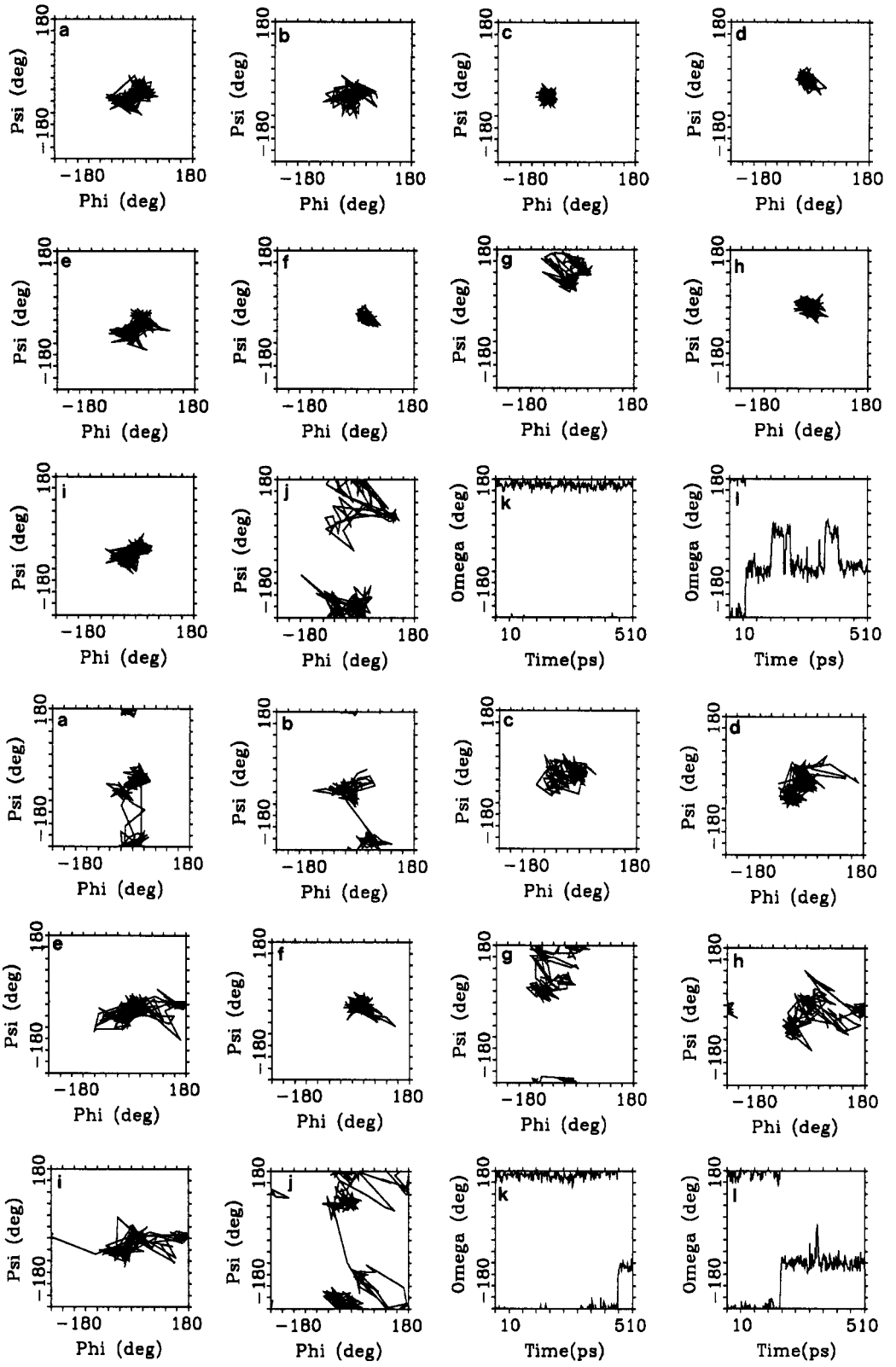

FIGURE 4: Instantaneous values of ϕ *vs* ψ and ω over the last 500 ps of restrained (upper panels) and free (lower panels) MD simulations of **I**. Panels correspond with the following glycosidic linkages and torsion angles: (a) GlcNAcβ1−4GlcNAc; (b) Manβ1−4GlcNAc; (c) Manα1−3Man; (d) GlcNAcβ1−2Manα1−3; (e) GlcNAcβ1−4Manα1−3; (f) GlcNAcβ1−4Manβ; (g) Manα1−6Man; (h) GlcNAcβ1−2Manα1−6; (i) GlcNAcβ1−4Manα1−6; (j) GlcNAcβ1−6Man; (k) ω for Manα1−6Man; (l) ω for GlcNAcβ1−6Man.

tially greater than the detection limit is that between GlcNAc 9 H-4 and Man 5 H-1 (2.1%), and this NOE could retrospectively be assigned with an experimental intensity of 2.0%. The remaining NOEs at or around the 1% limit could not be detected with certainty.

Small NOEs (close to the limit of detection) that were predicted from the model between protons on the B-face of GlcNAc 5′ and the B-face of GlcNAc 2 could not be observed experimentally. However, significant negative ^{1}H glycosylation shifts (Lemieux *et al.*, 1980; Bock *et al.*, 1986;

Table 2: Time-Averaged Glycosidic Bond Torsion Angles over the Last 500 ps of 510 ps restrained MD Simulation of I[a]

linkage	$\langle\phi\rangle$	$\langle\psi\rangle$
GlcNAc 2−GlcNAc 1	23 (28)	−19 (21)
Man 3−GlcNAc 2	24 (28)	−9 (20)
Man 4−Man 3	−50 (11)	−13 (12)
GlcNAc 9−Man 3	56 (12)	5 (10)
Man 4′−Man 3	19 (26)	112 (24)
GlcNAc 5−Man 4	18 (14)	34 (13)
GlcNAc 5′−Man 4′	28 (16)	31 (15)
GlcNAc 7−Man 4	14 (26)	−26 (19)
GlcNAc 7′−Man 4′	23 (52)	180 (64)
GlcNAc 10′−Man 4′	33 (25)	−10 (23)

[a] Angles are in degrees. RMS deviations are given in parentheses.

Table 3: Absolute NOEs between Proton Pairs not Included in the Modeling Constraints File but Which are Predicted from the Restrained MD Simulation

protons			protons		
from	to	NOE (%)	from	to	NOE (%)
H-1 (2)	$H\text{-}6_{proS}$ (1)	0.5	H-2 (4′)	$H\text{-}6_{proS}$ (3)	1.1
H-1 (2)	$H\text{-}6_{proR}$ (1)	0.2	H-2 (4′)	$H\text{-}6_{proR}$ (3)	0.4
H-3 (2)	H-3 (5′)	0.7	H-3 (4′)	H-5 (9)	1.2
H-3 (2)	H-5 (5′)	0.7	H-5 (4′)	H-5 (9)	1.0
H-5 (2)	H-5 (5′)	0.5	H-1 (5)	H-4 (9)	2.1
H-1 (3)	$H\text{-}6_{proR}$ (2)	0.7	H-3 (5)	H-2 (9)	0.9
H-1 (3)	$H\text{-}6_{proS}$ (2)	0.5	H-1 (7)	$H\text{-}6_{proR}$ (4)	1.3
H-2 (3)	$H\text{-}6_{proR}$ (2)	0.8	H-1 (7)	$H\text{-}6_{proS}$ (4)	0.7
H-2 (3)	$H\text{-}6_{proS}$ (2)	0.4	H-2 (7′)	H-3 (9)	0.4
H-2 (4′)	H-4 (3)	2.6			

Homans *et al.*, 1987; Jansson *et al.*, 1989) were observed for H-3 and H-5 of the terminal GlcNAc 5′ (but not for H-2, H-4, or either H-6), supporting the proposal that GlcNAc 5′ is folded back with the B-face in proximity to the glycan core.

DISCUSSION

The data above suggest that the majority of glycosidic linkages in the penta-antennary glycan exhibit limited torsional oscillations in solution. A notable exception is the GlcNAcβ1−6Man linkage, which is more highly disordered. In general, the glycosidic linkages in the penta-antennary glycan which are common to the biantennary bisected glycan occupy similar minimum energy regions of ϕ,ψ space (Rutherford & Homans, 1994) but are more highly ordered in the former as a direct result of steric hindrance due to the additional substituents. As a result, the "global minimum" conformation (Figure 3) is a good approximation to the average solution conformation. It is important to recognize that the NOE restraints provide a small contribution to compensate for the poor performance of the molecular mechanics force-field in regions away from the global energy minima. As discussed previously, these limitations are not unique to the current force field, and reflect the difficulty of parametrizing for flexible polar molecules in solution (Rutherford & Homans, 1994). Since the restraint energy is low in the MD simulation, and the structure occupies the global minimum energy well, the restraints are not forcing the structure to adopt a high-energy virtual conformation that is consistent with NMR data but lacks physical meaning.

In the native glycan, the extent of galactosylation of the nonreducing terminal GlcNAc residues is highly limited: ~20% of penta-antennary chains bear Galβ in 1−4 linkage to the GlcNAcβ1−4Manα1−6 unit, ~13% bear Galβ in 1−4 linkage to the GlcNAcβ1−4Manα1−3 unit, ~8% contain both, and less than 2% bear Galβ in 1−4 linkage to either the GlcNAcβ1−2Manα1−6 or GlcNAcβ1−2Manα1−3 units (Yamashita *et al.*, 1982). There is no galactosylation of the GlcNAcβ1−6Manα1−6 unit. This cannot be rationalized in terms of a simple model based upon steric hindrance: While none of the terminal GlcNAc residues is buried in the three-dimensional structure of the glycan, both GlcNAc residues on the Manα1−3 antenna and the GlcNAcβ1−4 and GlcNAcβ1−6 residues on the Manα1−6Man antenna would be predicted from Figure 3 to be the most accessible to a galactosyl transferase. Taken together, these data suggest either that different galactosyl transferases are required for full galactosylation of the penta-antennary glycan, and these are expressed at various levels of activity in hen oviduct, or that *N*-acetyllactosamine synthetase adds galactose to the terminal GlcNAc residues at different rates, as suggested by Yamashita et al. (1982). In the latter case it is difficult to reconcile such differences in rates with the three-dimensional structure of the glycan, but, however, the protein itself may influence the rate of galactosylation. It should be possible to distinguish between these possibilities by galactosylation with *N*-acetyllactosamine synthetase of the penta-antennary glycan *in vitro* both free and in covalent association with the parent glycoprotein, followed by detailed sequence analysis of products. Such studies are currently in progress.

ACKNOWLEDGMENT

We thank Dr. Angela Mehlert for the electrospray mass spectrometry.

SUPPORTING INFORMATION AVAILABLE

Virtually complete proton resonance assignments and glycosylation shifts for **I** (1 page). Ordering information is given on any current masthead page.

REFERENCES

Bock, K., Brignole, A., & Sigurskjold, B. W. (1986) *J. Chem. Soc., Perkin Trans. 2*, 1711−1713.
Brisson, J.-R., & Carver, J. P. (1983) *Biochemistry 22*, 3680−3686.
Homans, S. W. (1990) *Biochemistry 29*, 9110−9118.
Homans, S. W. (19930 Conformational studies on oligosaccharides in *Molecular Glycobiology*, Frontiers in Molecular Biology Series, (Fukuda, M., Ed.) Oxford University Press, pp 230−257.
Homans, S. W., & Forster, M. (1992) *Glycobiology 2*, 143−151.
Homans, S. W., Dwek, R. A., Boyd, J., Mahmoudian, M., Richards, W. G., & Rademacher, T. W. (1986) *Biochemistry 25*, 6342−6350.
Homans, S. W., Dwek, R. A., & Rademacher, T. W. (1987) *Biochemistry 26*, 6553−6560.
Jansson, P.-E., Kenne, L., & Widmalm, G. (1989) *Carbohydr. Res. 188*, 169−191.
Kogelberg, H., & Rutherford, T. J. (1994) *Glycobiology 4*, 49−57.
Lemieux, R. U., Bock, K., Delbaere, L. T. J., Koto, S., & Rao, V. S. (1980) *Can. J. Chem. 38*, 631−653.
Nishida, Y., Hori, H., Ohrui, H., & Meguro, H. (1987) *J. Carbohydr. Chem. 7*, 239−250.
Patel, T., Bruce, J., Merry, A., Bigge, C., Wormald, M., Jaques, A., & Parekh, R. (1993) *Biochemistry 31*, 679−693.
Rutherford, T. J., & Homans, S. W. (1994) *Biochemistry 33*, 9606−9614.
Rutherford, T. J., & Homans, S. W. (1995) *J. Magn. Reson. B 106*, 10−13.

Rutherford, T. J., Partridge, J., Weller, C. T., & Homans, S. W. (1993) *Biochemistry 32*, 12715−12724.

Rutherford, T. J., Spackman, D. G., Simpson, P. J., & Homans, S. W. (1994) *Glycobiology 4*, 59−68.

Singh, U. C., Weiner, P., Caldwell, J., & Kollman, P. A. (1986) *AMBER 3.0*, University of California, San Francisco, CA.

Takasaki, S., Ikehara, H., & Kobata, A. (1980) *Biochem. Biophys. Res. Commun. 92*, 735−742.

Tropp, J. (1980) *J. Chem. Phys. 72*, 6035−6043.

Varki, A. (1993) *Glycobiology 3*, 97−130.

Vliegenthart, J. F. G., Dorland, L., & van Halbeek, H. (1983) *Adv. Carbohydr. Chem. Biochem. 41*, 209.

Weiner, S. J., Kollman, P. A., Case, D. A., Singh, C. S., Ghio, C., Alagona, G., Profeta, S. P., & Weiner, P. (1984) *J. Am. Chem. Soc. 106*, 765−784.

Yamashita, K., Kamerling, J. P., & Kobata, A. (1982) *J. Biol. Chem. 257*, 2809−2814.

Yamashita, K., Koide, N., Endo, T., Iwaki, Y., & Kobata, A. (1989) *J. Biol. Chem. 264*, 2415−2423.

BI951368P